



POLİTEKNİK DERGİSİ

*JOURNAL of POLYTECHNIC*

ISSN: 1302-0900 (PRINT), ISSN: 2147-9429 (ONLINE)

URL: <http://dergipark.org.tr/politeknik>



# Evaluation of dynamic response variability in aluminum honeycomb sandwich panels using PCE and Kriging-based metamodel

*Alüminyum petek sandviç panellerde dinamik tepki değişkenliğinin PCE ve Kriging tabanlı meta-model kullanılarak değerlendirilmesi*

*Authors (Yazarlar): Akın OKTAV<sup>1</sup>, Murat Alper BAŞARAN<sup>2</sup>*

ORCID<sup>1</sup>: 0000-0001-5983-3953

ORCID<sup>2</sup>: 0000-0001-9887-5531

**To cite to this article:** Oktav A. and Başaran M. A., “Evaluation of dynamic response variability in aluminum honeycomb sandwich panels using PCE and Kriging-based metamodel”, *Journal of Polytechnic*, \*(\*) : \*, (\*).

**Bu makaleye şu şekilde atıfta bulunabilirsiniz:** Oktav A. ve Başaran M. A., “Alüminyum petek sandviç panellerde dinamik tepki değişkenliğinin PCE ve Kriging tabanlı meta-model kullanılarak değerlendirilmesi”, *Politeknik Dergisi*, \*(\*) : \*, (\*).

**Erişim linki (To link to this article):** <http://dergipark.org.tr/politeknik/archive>

**DOI:** 10.2339/politeknik.1498060

# Evaluation of Dynamic Response Variability in Aluminum Honeycomb Sandwich Panels Using PCE and Kriging-Based Metamodel

## Highlights

- ❖ The response of the core cell walls is particularly decisive at high frequencies and cannot be captured when the core is taken as an equivalent volume.
- ❖ The uncertainties in the core structure mostly originated from the inhomogeneity of adhesive fillets.
- ❖ The variability at low frequencies is due to the facing sheets, while the variability at high frequencies is dominated by the core.

## Graphical Abstract

In this work, the dynamic response variability in 35 aluminum honeycomb sandwich panel samples is examined using a PCE and Kriging-based metamodel.

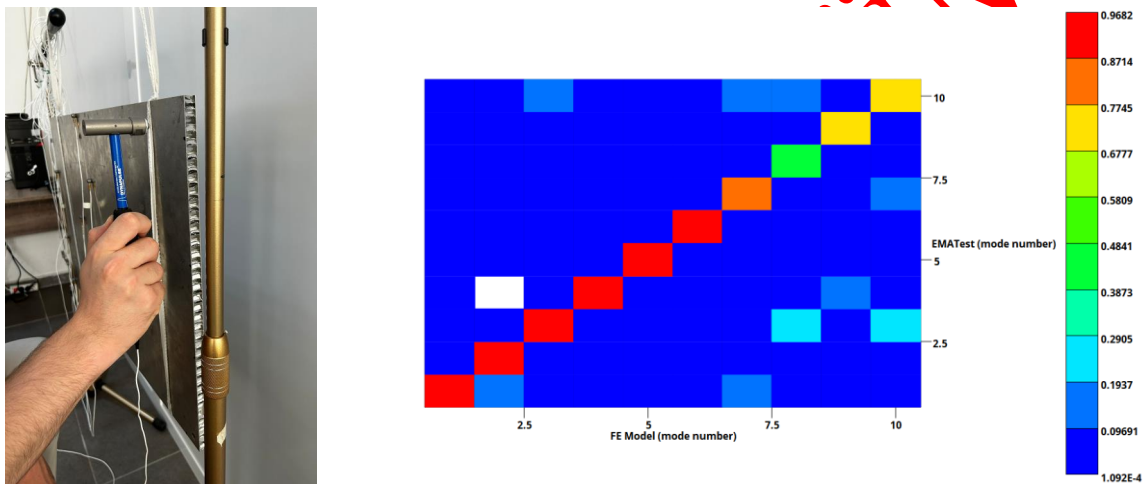


**Figure.** Experimental modal analysis of aluminum honeycomb sandwich panels

## Aim

To model the dynamic response variability in commercial aluminum honeycomb sandwich panels.

## Design & Methodology

The experimental data are acquired through experimental modal analysis techniques. The computational model is constructed using shell modeling. The modal frequency values obtained for the samples are compared with the computational results and deviations are referred to as errors.

## Originality

A data-driven meta-model called PCE-Kriging is created to express the relationship between error and the stochastic variables.

## Findings

The results show that the variability at low frequencies is due to the facing sheets, while the variability at high frequencies is dominated by the core.

## Conclusion

The uncertainties in the core structure mostly originated from the inhomogeneity of adhesive fillets which alter the effective cell wall thickness

## Declaration of Ethical Standards

The authors of this article declare that the materials and methods used in this study do not require ethical committee permission and/or legal-special permission.

# Evaluation of Dynamic Response Variability in Aluminum Honeycomb Sandwich Panels Using PCE and Kriging-Based Metamodel

*Araştırma Makalesi / Research Article*

Akın OKTAV<sup>1\*</sup>, Murat Alper BAŞARAN<sup>2</sup>

<sup>1</sup>Department of Mechanical Engineering, Alanya Alaaddin Keykubat University, Antalya 07425 Türkiye

<sup>2</sup>Department of Industrial Engineering, Alanya Alaaddin Keykubat University, Antalya 07425 Türkiye

(Geliş/Received : 08.06.2024 ; Kabul/Accepted : 29.04.2025 ; Erken Görünüm/Early View : 06.05.2025 )

## ABSTRACT

The aim of this study is to model the dynamic response variability in commercial aluminum honeycomb sandwich panels. An experimental modal analysis is performed on 35 identical commercial AHSPs. Based on 10,000 samples, a computational model is constructed according to the estimated weight of the panel. The modal frequencies of the 35 samples for the first 10 flexible modes are compared with the computational results and deviations are referred to as errors. The thickness of the facing sheets and thickness of the cell wall of the core are considered as sources of uncertainty. A data-driven meta-model called PCE-Kriging is created.

**Keywords:** Kriging, modal analysis, polynomial chaos expansion (PCE), uncertainty quantification, variability.

## Alüminyum Petek Sandviç Panellerde Dinamik Tepki Değişkenliğinin PCE ve Kriging Tabanlı Meta-Model Kullanılarak Değerlendirilmesi

### ÖZ

Bu çalışmanın amacı, ticari alüminyum petek sandviç panellerdeki (APSP) dinamik tepki değişkenliğini modellemektir. Özdeş 35 ticari APSP üzerinde deneysel modal analiz çalışması gerçekleştirilmiştir. Panelin tahmini ağırlığına göre 10.000 örnek temel alınarak bir hesaplamalı model oluşturulmuştur. İlk 10 esnek mod için 35 numunenin deneysel modal frekansları, deterministik hesaplama modelinin sonuçlarıyla karşılaştırılmış ve sapmalar hata olarak nitelenmiştir. Kaplama levhalarının kalınlıkları ve çekirdek hücre duvarının kalınlığı belirsizlik kaynakları olarak kabul edilmiştir. Hata ve stokastik değişkenler arasındaki ilişkiyi ifade etmek için PCE-Kriging adı verilen veri güdümlü bir meta-model oluşturulmuştur. Sonuçlar, düşük frekanslardaki değişkenliğin kaplama tabakalarından kaynaklandığını, yüksek frekanslardaki değişkenliğin ise çekirdek tarafından domine edildiğini göstermektedir.

**Anahtar Kelimeler:** Kriging, modal analiz, çokterimli kaos açılımı, belirsizlik sayısallaştırma, değişkenlik.

### 1. INTRODUCTION

Aluminum honeycomb sandwich panels (AHSPs) have been commonly designed and implemented due to their benefits. Some of these benefits include high strength to weight ratio, crashworthiness, energy absorption, and effective acoustic insulation [1–5]. AHSPs are used in the rail systems, ship construction, automotive, and aviation industries [6–14]. Apart from specialized applications such as artificial satellite construction [15–17], commercial AHSPs are generally used in industrial applications.

Due to manufacturing uncertainties in commercial AHSPs, there may be significant variances between panels considered identical. It is important to consider these variances when designing or testing any engineering structure where AHSPs are employed. The term variability can be categorized as inter variability and intra variability. Inter variability is defined as variances

in the response of identical systems under the same environmental conditions while intra variability as variances in the response of a system under different environmental conditions [18, 19]. Intra variability arises due to environmental parameters such as different operating conditions and different ambient temperatures. Inter variability arises occasionally due to production errors, assembly procedure and tolerances in modeling. The terms variability and uncertainty are sometimes used interchangeably, leading to confusion [20, 21]. Variability in this work is related to aleatory uncertainty rather than epistemic uncertainty. Depending on the aleatory uncertainties, the dynamic response of the AHSPs is said to be stochastic. Uncertainties in material properties, geometric and physical parameters also cause variability. In the commercial AHSPs the sources of uncertainty are the geometry heterogeneity and the effective mechanical properties of materials which are

\*Sorumlu Yazar (Corresponding Author)

e-Posta : akin.oktav@alanya.edu.tr

mostly altered due to the presence of adhesives used for assembling the AHSPs [22].

Engineering structures are often exposed to dynamic loading [23, 24]. In the relevant literature it is shown that the dynamic response of honeycomb structures is sensitive to geometric variables [25–27]. Besides the geometric variables, the mechanical properties of materials also affect the dynamic response results which are shown in model update studies [22, 28]. The response of AHSPs to dynamic loading is an important concern that must be validated at the design stage. The aim of the current study is to model the dynamic response variability in commercial AHSPs.

Geometrical irregularities occur in the honeycomb cells due to the manufacturing procedure. These irregularities cause uncertainties in the mechanical performance of the panels. Zhao et al. developed a fast Fourier transform based method to predict the in-plane elastic properties of irregular hexagonal cores [29]. Dey et al. proposed multivariate adaptive regression splines-based uncertainty quantification method for composite sandwich structures [30]. According to the researchers, this approach effectively replaces the Monte Carlo based stochastic models for sandwich composite structures with a computationally efficient model, making the overall uncertainty quantification process much more cost-effective. Zhang et al. [31] conducted a computational study on a honeycomb sandwich structure to attain its real strength boundary at failure considering the randomness of its parameters as characterized by Latin hypercube sampling using Matlab. Lajili et al. [32] investigated the wave propagation features in a sandwich panel with honeycomb core over a large frequency domain in presence of uncertainties. They use the generalized polynomial chaos method with Latin hypercube sampling. In a study aiming to increase the strength of a honeycomb structure [33], grey relational grade is assigned to three objective functions consisting of von Mises stresses computed according to three different standards. The results of a uniform design of experiment and grey relational grades were used in surrogate models created using Kriging interpolation.

Polynomial chaos expansion (PCE) and Kriging-based metamodels are often used in reliability-based design optimization (RBDO) studies and many successful results are reported in literature [34–36]. This metamodeling algorithm utilizes the advanced techniques of PCE [37, 38] and Kriging (Gaussian process modeling) [39–41]. To model the dynamic response variability in commercial AHSPs, a PCE and Kriging-based metamodel is adopted in this work. The structure of this paper is as follows. To obtain modeling data, 35 samples measuring 750mm×500mm×15 mm are subjected to experimental modal analysis as explained in Section 2. In Section 3, fundamental notions of the three surrogate models, generalized polynomial chaos expansion (gPCE), Kriging metamodeling, and PCE-Kriging, are briefly explained and then the section copes with how these models are implemented for various

engineering and applied science problems in literature. The construction of the data-driven meta-model called PCE-Kriging for the AHSP is introduced in Section 4. Finally, a few brief conclusions are drawn in the last section.

## 2. EXPERIMENTAL MODAL ANALYSIS

Important dynamic properties are the natural frequencies, mode shapes, and damping ratios. Experimental modal analysis (EMA) is a testing and analysis procedure used to determine these dynamic properties through measured frequency response functions (FRFs). The experimental procedure includes data collection and analysis of the samples. The analyzed data makes it possible to examine the impact of system properties on the response. To obtain reliable test data, the excitation (input) and response (output) locations must be successfully determined through a pre-test model [42, 43].

To build a pre-test model, a computational model is first constructed in Siemens Simcenter 3D. The first step in preparing the model is to draw the core structure. The most important detail to note in the drawing is that some of the joints in the core structure have double cell walls, not single. Any hexagonal cell has a manufacturing-induced double cell wall on two sides. Since glue will be used at the joints, tolerance values should be adjusted accordingly. Since the material is isotropic, it is realistic to create a mesh structure with two-dimensional elements. Since the mesh structure will be created using the shell/shell/shell (SSS) approach with two-dimensional elements, the midsurface of the entire geometry is extracted, where a section is shown in Figure 1 [22]. For a detailed discussion on VVV, SVS and SSS modeling the interested readers are referred to Ref. [44]. The dimensions of the AHSP model and the mechanical properties of the materials are tabulated in Table 1 and Table 2, respectively. The commercial AHSP is obtained from Altigen Co. [45]. Total number of elements and nodes are 189,452 and 348,726, respectively.

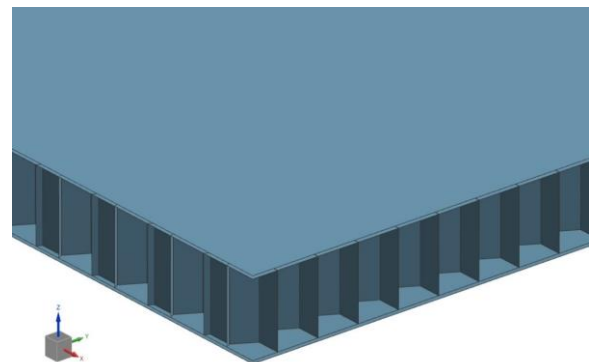


**Figure 1.** The midsurfaces of CAD used in the modeling

To extract the eigenfrequencies and eigenvectors of the panel, the eigenvalue problem is solved using Lanczos algorithm built-in Siemens Simcenter3D. Then, a pre-test model is created. The pre-test model is used to determine the excitation and response locations at which accelerance FRFs (a/F) will be acquired in the

experiment. The critical node locations to be measured are determined with the min-MAC algorithm.

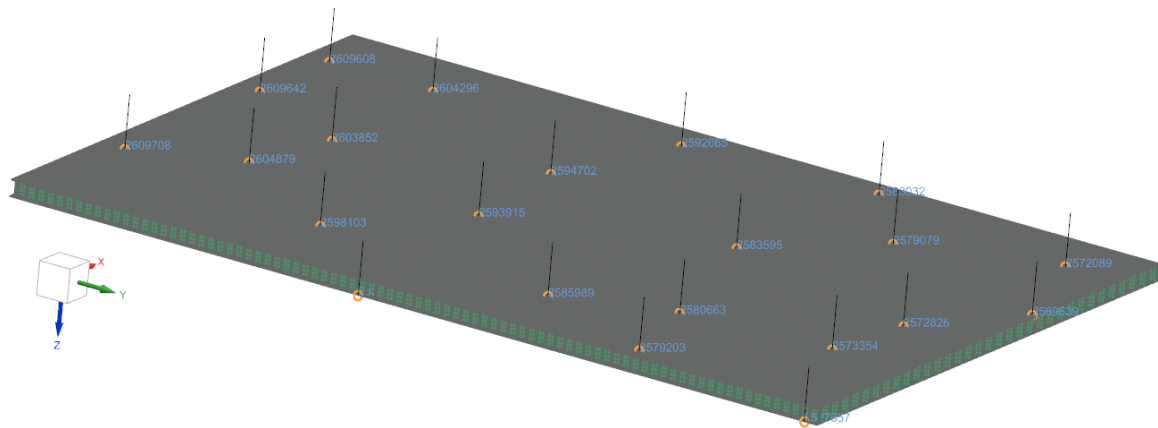
**Table 1.** The dimensions of the AHSP

Components	Parameter	Dimension (mm)
Facing sheets	Length ( $l$ )	750
	Width ( $w$ )	500
	Height ( $h$ )	1
Core	Cell side length ( $l_c$ )	5
	Cell radius ( $R$ )	8.66
	Cell wall thickness ( $t$ )	0.05
	Height ( $h$ )	13

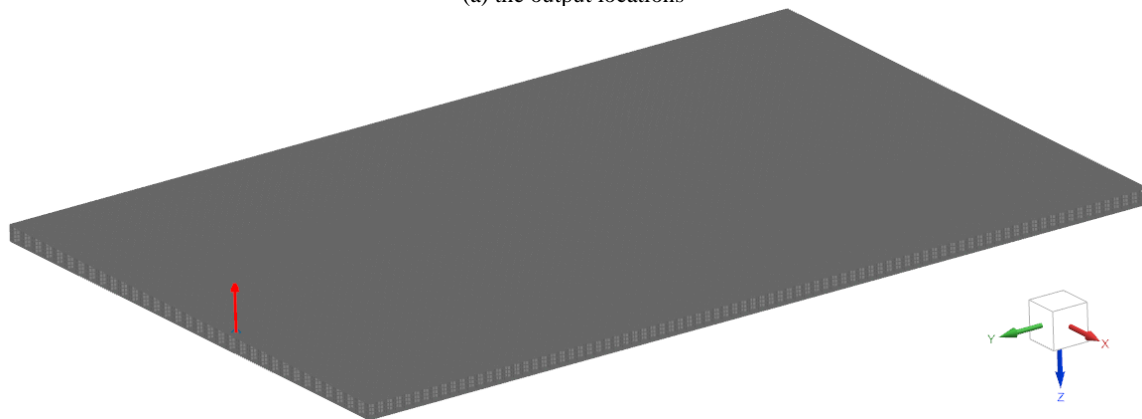
and three dof for the triaxial sensor. The dof are added by selecting one at a time from the candidate set. The algorithm keeps track of a subset of off-diagonal MAC terms during the selection process. This subset starts with the largest available diagonal term of the MAC matrix. Other terms are added to the watchlist as they become the largest diagonal term of the MAC matrix. Optimum excitation locations are determined by the normal mode indication function (NMIF). Through the pre-test model with Guyan reduction, 21 output locations and 1 input location are identified. The locations are shown in Figure 2.

**Table 2.** Mechanical properties of materials

Material	Geometry	Elastic modulus (MPa)	Poisson's ratio	Density (kg/m <sup>3</sup> )
Aluminum 5754	Facing sheet	70,300	0.33	2,670
Aluminum 3005	Core	69,000	0.34	2,700
Polyurethane hard	Adhesive	900	0.40	1,200



(a) the output locations



(b) the input location

**Figure 2.** Sensor locations determined through pre-test analysis.

The algorithm uses the SOL103 solution file to determine the node locations such that the diagonal terms in the autocorrelation modal assurance criterion (Auto-MAC) matrix are 1 and the diagonal terms are 0.2 or less. The algorithm starts with the required set of degrees-of-freedom (dof) and adds one dof for the uniaxial sensor

A Sinus analyzer, a Dytran roving hammer and Dytran uniaxial accelerometers are used to measure the FRFs from the 21 determined sensor locations. The experimental data are obtained under free boundary conditions. To achieve the free boundary conditions, elastic ropes are used where shown in Figure 3.



a) AHSP samples



b) Modal test

**Figure 3.** Modal test of 35 AHSP samples

The frequency range is 1.2 kHz, and the number of spectral lines is 3,200. The experimental raw data is processed through nCode software using a linear least squares regression fit. The variation in the dynamic response of AHSPs in terms of flexible modal frequency values is shown in Figure 4. The dimensions and weights

of the samples were measured before the modal test. It was observed that the weights of the samples, which were assumed to be identical, were not equal. The weights of the samples are tabulated in Table 3. From a commercial point of view, the samples are considered to be identical. Since the samples were precision cut from larger

**Table 3.** The weights of AHSP samples (error term = weight of the panel – average)

Panel #	Weight (gram)/error	Panel #	Weight (gram)/error
1	2,461.5/-45.5	19	2,498.2/-8.8
2	2,487.3/-19.7	20	2,548.0/41
3	2,516.7/9.7	21	2,622.0/115
4	2,433.0/-74	22	2,505.0/-2
5	2,472.9/-34.1	23	2,646.3/139.3
6	2,419.7/-87.3	24	2,560.7/53.7
7	2,525.4/18.4	25	2,511.7/4.7
8	2,397.1/-109.9	26	2,468.6/-38.4
9	2,491.6/-15.4	27	2,492.0/-15
10	2,568.3/61.3	28	2,593.2/86.2
11	2,537.1/30.1	29	2,586.2/79.2
12	2,387.0/-120	30	2,502.4/-4.6
13	2,551.0/44	31	2,524.5/17.5
14	2,460.4/-46.6	32	2,465.8/-41.2
15	2,410.6/-96.4	33	2,505.8/-1.2
16	2,519.8/12.8	34	2,479.0/-28
17	2,498.7/-8.3	35	2,643.5/136.5
18	2455.0/-52		
<b>average</b>	<b>2,507.0</b>	<b>std. deviation</b>	<b>63.94</b>

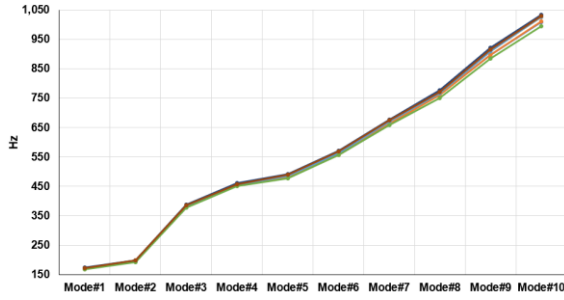


**Figure 4.** The variation in the dynamic response of AHSPs in terms of modal frequency values (Experimental results)

commercial panels measuring 3,000 mm × 1,500 mm, it was observed that the samples met the specified dimensions of 750 mm × 500 mm × 15 mm. Precise measurements with calipers showed that the facing sheet heights were not exactly 1.00 mm at each position along the panel, but had a height between 0.96 mm–1.03 mm. It is noted as a source of uncertainty to be evaluated in the modeling phase (see Section 4). In order to study the core structure and adhesive state, a cut piece supplied with the specimens was studied. The cell wall thickness ( $t$ ) was measured as 50 microns with a digital caliper. It was observed that the corners of the honeycomb cells were not ideal as assumed in the drawing but had a rounded appearance. This is one of the uncertainties associated with manufacturing. Also, as expected, the distribution of the cell structure is not homogeneous. The main element of uncertainty to consider is the condition of the adhesive layers. The adhesive flows during manufacturing, creating a fillet-shaped residue between the cell walls and facing sheets. After curing, the adhesive fillet layer hardens and alters the buckling strength of the thin cell walls, as analyzed in detail in a previous study [22]. This is another source of uncertainty worth considering in the modeling phase (see Section 4). The weight of the computational model is the same as the average weight of the panels. When the mentioned density values are assigned, the weight of the panel in the computational model is 2,507.0 grams. The mode number and frequency values obtained from the modal test results are given in Section 4, where a data-driven meta-model called PCE-Kriging for the AHSP is introduced. But before that, the following section briefly explains the basic concepts of the three surrogate models - generalized polynomial chaos expansion (gPCE), Kriging metamodeling and PCE-Kriging - and then discusses how these models are implemented to engineering solutions and applied science problems in literature.

### 3. METAMODELING

This section is composed of two main subsections: while the first part (Section 3.1) deals with briefly explaining the fundamental notions of the three surrogate models, the second part (Section 3.2) copes with how these

models are implemented for various engineering and applied science problems in literature.

#### 3.1. Surrogate Models

##### 3.1.1. Generalized polynomial chaos expansion (gPCE)

The computational burden of simulations in engineering and applied sciences is huge. Thus, more effective methods are suggested in the literature. These methods are based on quantifying intrinsic uncertainty between input variables and output variables by representing input variables as well-known probability distributions such as Gaussian, Weibull, and Gamma. This approach is called metamodeling or surrogate modeling entitled generalized polynomial chaos expansion (gPCE) that generates an approximation function for the computationally known model or fits dataset of real input values and stochastic output variables produced by simulation methods, e.g., Monte Carlo. Thus, spectral representation on a suitably constructed basis of orthogonal polynomials is generated to represent a model between a set of input variables and an output variable as follows:

$$E(Y^2) = \int M^2(\mathbf{x}) f_{\mathbf{x}}(\mathbf{x}) d\mathbf{x} < \infty \quad (1)$$

where  $\mathbf{x} \in D_{\mathbf{x}}$  denotes the function domain and  $\mathbf{x} = (x_1, x_2, \dots, x_n)^T$  represents  $n$ -dimensional input vector,  $E(\cdot)$  represents the expected value operator,  $f_{\mathbf{x}}(\mathbf{x})$  denotes  $n$ -dimensional joint probability density function with independent random variables. So, gPCE is defined as follows:

$$Y = M(\mathbf{X}) = \sum_{\alpha \in N^M} (\gamma_{\alpha} \psi_{\alpha}(\mathbf{X})) \quad (2)$$

where the term  $\psi_{\alpha}(\mathbf{X})$  in Equation (2) denotes multivariate polynomials basis orthonormal to  $f_{\mathbf{x}}(\mathbf{x})$ ,  $\alpha \in N^M$  shows a multi-index identifying multivariate polynomials' coefficients,  $\psi_{\alpha}(\mathbf{X})$ , and the coefficients are denoted by  $\gamma_{\alpha}$ . Since the truncation of Equation (2) is required at some power, Equation (2) is rewritten approximately as follows:

$$M(\mathbf{X}) \approx M^{PCE}(\mathbf{X}) = \sum_{\alpha \in A} (\gamma_{\alpha} \psi_{\alpha}(\mathbf{X})) \quad (3)$$

where  $A \subset N^M$  denotes the set of picked multi-indices of multivariate polynomials. Univariate orthonormal polynomials,  $\Phi_k^{(i)}(x_i)$ , are used to construct  $\psi_{\alpha}(\mathbf{X})$  polynomials basis as follows:

$$\begin{aligned} \langle \Phi_j^{(i)}(x_i) \Phi_k^{(i)}(x_i) \rangle &= \\ \int \Phi_j^{(i)}(x_i) \Phi_k^{(i)}(x_i) f_{x_i}(x_i) dx_i &= \delta_{jk} \end{aligned} \quad (4)$$

where superscript  $i$ , subscripts  $j$ , and  $k$ ,  $\delta_{jk}$ , and  $f_{x_i}(x_i)$ , represent orthogonal polynomials concerning  $i$ th input, corresponding polynomial degrees for  $j$  and  $k$ , the Kronecker symbol,  $i$ th input variable probability mass or density function.

##### 3.1.2. Kriging metamodeling

Kriging *aka* Gaussian process modeling assumes the realizations of the output variable stemming from the Gaussian random process defined in Equation (5) [46]

$$M(\mathbf{X}) = M^K(\mathbf{X}) = \boldsymbol{\beta}^T f(\mathbf{x}) + \sigma^2 Z(\mathbf{x}) \quad (5)$$

where the trend also called the mean of the Gaussian process is denoted by  $\beta^T f(\mathbf{x})$ ,  $\sigma^2$  is called variance and,  $Z(\mathbf{x})$  represents a stationary Gaussian process whose means and variance are 0 and 1, respectively.

Since Kriging is employed to construct an approximation function and interpolation for a given computationally known function or a design matrix of input and out variables, a simple global error measurement showing the meta-model's precision is not available due to Kriging's interpolating attributions. Leave-one-out (LOO) is a method to globally measure errors defined by Equation (6) [46].

$$Err_{LOO}^K = \frac{1}{N} \sum_{i=1}^N (y^{(i)} - \mu_{y(\cdot)}(X^{(i)}))^2 \quad (6)$$

where the first term in the parathesis is the response value and the next term is the estimated value using the Kriging model.

### 3.1.3. PCE-kriging

PCE-Kriging is a surrogate model that combines both gPCE and Kriging defined by Equation (7).

$$M(\mathbf{X}) \approx M^{PCK}(\mathbf{X}) = \sum_{\alpha \in A} (y_{\alpha} \psi_{\alpha}(\mathbf{X})) + \sigma^2 Z(\mathbf{x}) \quad (7)$$

where  $y_{\alpha} \psi_{\alpha}(\mathbf{X})$ ,  $A$ , and  $Z(\mathbf{x})$  represent a weighted sum of orthonormal polynomials called the average of the Gaussian process, the index set of the polynomials, and a stationary Gaussian process whose means and variance are 0 and 1, respectively.

Two different frameworks are used in PCE-Kriging which are called sequential and optimal, and they are abbreviated as SPCE-Kriging and OPCE-Kriging. Santner et al. [46] suggest that OPCE-Kriging is superior to SPEC-Kriging when the experimental design is under consideration since it has the lowest generalized statistical error.

### 3.2. Implementation of PCE-Kriging Surrogate Model

The differences observed in the modal frequency values obtained from the experimental model and from the computational model are termed as errors. The errors are assumed to stem from the stochastic properties of the AHSP samples. As analyzed throughout the study, it is assumed that the samples are identical, but they are not. It is more realistic to model uncertainty to come up with a reliable solution. Thus, one can assume that the deviations observed between the experimental and computational results originated from uncertainties associated with the geometric properties of honeycomb panels, which are determined as the thicknesses of the upper facing sheet, core structure, and the lower facing sheet.

The surrogate model called gPCE has been implemented for simulation-based models as alternative easy-to-implement models and generated predictions [47–50]. Hadj et al. [47] dealt with designing the parameters of a wind turbine's two-stage gearbox. Umesh and Ganguli [48] researched the materials' uncertainty impact to control the vibration of smart composite plates by utilizing piezoelectric sensors. Azrar et al. [49] examined

the impact of uncertain parameters affecting viscoelastic Carbon Nanotubes (CNT) dynamical behavior when a viscous fluid is conveyed in it. Peng et al. [50] investigated composite laminated plates by using micro and macro parameters based on random and interval variables to represent uncertainty. Chen et al. [51] suggested a method to design underwater vehicles using composite materials whose mechanical properties are represented by PCA. On the other hand, the PCE-Kriging method has proven itself in several engineering modeling processes. Aversano et al. [52] proposed a method that predicts 2D combustion data when unexplored operating conditions are under consideration. García-Macías and Ubertini [53] proposed a method that estimates automatic damage identification for large-scale structures. Sinou and Denimal [54] suggested a method that tracks traverse cracks and pinpoints them in rotating components using the PCE-Kriging method based on uncertain parameters of position and depth.

## 4. DATA ANALYSIS

In the analysis, 3 geometric variables of AHSPs are considered as sources of uncertainty; these are the thicknesses of the upper and lower facing sheets and the cell wall thickness of core. Their distributions are assigned as follows: upper and lower facing sheets are uniformly Gaussian with mean 1 and standard deviation 0.05, and the core structure is Gaussian with mean 0.9 and standard deviation 0.05. These distributions are determined through experimental measurements and computational analysis. Precise measurements with calipers showed that the facing sheet heights were not exactly 1.00 mm at each position along the panel, but had a height between 0.96-1.03 mm. Computational analysis performed on one of the AHSP samples which is selected according to the statistical analysis revealed that even the cell wall thickness of the core elements are 50  $\mu\text{m}$ , the effective cell wall thickness ( $t_c$ ) is computed as 92  $\mu\text{m}$ , as shown and explained in the previous work [22]. The  $t_c$  value is different from the actual one. This is mainly due to the adhesive fillets that form at the bonding interface of facing sheets and the honeycomb core during the manufacturing process. The data-driven meta-model called PCE-Kriging is constructed. The first 10 flexible modal frequency values of 35 AHSP samples (experimental values) and the results of the computational model are tabulated in Table 4. Error values between each AHSP sample and the computational model for each modal frequency are tabulated in Table 5.

Furthermore, 10,000 samples are run to find the estimated average weight of AHSP. The outcomes are tabulated in Table 6. All calculations are performed with SPSS version 27.0. Since the bias value is too small, the estimated weight of 2,507.0 grams is used in the computational model.

In the case of AHSPs, various intrinsic properties can lead to uncertainties. These uncertainties can be

**Table 4.** The first 10 flexible modal frequency values of 35 AHSP samples and the computational model

Sample #	Modal frequencies									
	1	2	3	4	5	6	7	8	9	10
1	171.20	195.20	382.90	455.50	482.10	561.20	667.60	767.10	891.60	1,018.80
2	169.90	195.30	379.20	455.30	483.10	563.40	663.40	761.40	896.90	1,008.90
3	169.70	193.80	378.50	451.90	481.10	556.70	662.70	760.20	897.40	1,010.60
4	172.40	197.60	384.40	459.40	489.00	566.70	672.00	770.00	913.30	1,025.10
5	170.40	196.00	382.60	454.50	486.10	563.50	671.00	765.80	909.00	1,025.80
6	170.40	196.00	382.60	454.50	486.10	563.50	671.00	765.80	909.00	1,025.80
7	168.60	192.80	376.60	449.70	476.30	555.90	657.60	750.30	884.10	995.20
8	173.80	198.80	387.50	460.60	491.20	571.30	676.00	775.40	921.00	1,033.10
9	172.00	197.80	385.20	457.30	489.30	567.90	674.00	769.90	914.30	1,028.40
10	169.60	194.70	379.60	449.80	482.60	560.10	665.90	761.60	907.90	1,018.60
11	172.20	197.60	383.80	455.10	491.40	568.00	675.70	768.20	926.00	1,033.90
12	174.10	198.00	385.90	461.40	489.70	571.00	674.60	772.30	914.10	1,026.40
13	169.00	192.60	377.90	451.40	476.10	557.90	659.60	755.50	884.10	1,001.00
14	170.40	194.20	380.30	456.60	480.90	560.60	663.50	760.90	890.20	1,005.90
15	172.80	172.80	385.30	459.30	487.00	568.90	672.90	769.70	906.10	1,023.20
16	170.20	193.70	378.10	450.90	482.20	560.20	663.90	757.80	899.50	1,012.10
17	170.90	196.20	382.90	453.50	484.30	566.00	669.10	765.40	911.70	1,020.70
18	171.40	195.90	381.30	454.00	484.40	565.50	666.10	762.20	899.80	1,014.00
19	169.20	194.70	379.50	453.60	482.20	559.70	663.20	760.90	897.90	1,010.20
20	167.40	191.80	374.90	447.60	476.10	552.20	656.70	752.10	885.70	999.40
21	167.70	190.50	373.00	445.70	473.40	550.60	653.00	746.80	885.20	998.30
22	168.80	192.70	377.90	450.60	476.30	557.20	658.90	752.20	888.50	1,003.00
23	166.90	189.40	372.80	445.00	469.40	549.30	649.00	745.50	872.30	990.60
24	168.40	193.20	376.40	451.40	477.60	558.20	655.10	756.20	892.20	998.90
25	160.20	194.70	378.10	454.10	482.00	561.80	662.00	758.70	897.50	1,005.50
26	169.60	195.50	380.70	452.30	487.70	562.80	665.90	760.80	906.00	1,014.60
27	169.70	195.10	379.20	451.80	485.20	562.00	666.40	760.10	906.40	1,015.40
28	168.70	191.00	374.60	445.80	477.00	556.40	659.00	749.10	884.60	1,002.10
29	168.40	191.80	376.00	446.90	477.50	556.50	661.10	752.00	893.80	1,008.00
30	170.10	195.50	380.00	451.90	485.20	562.50	667.00	763.60	913.40	1,022.00
31	170.10	194.30	381.50	#AD?	480.10	560.00	665.20	760.60	898.20	1,014.20
32	172.00	197.40	384.80	457.60	487.90	572.80	672.30	767.60	920.10	1,023.70
33	170.40	195.50	378.60	455.10	483.70	566.10	663.20	759.20	908.00	1,007.90
34	171.00	196.10	382.00	453.80	484.90	565.50	668.90	763.60	908.40	1,016.60
35	168.10	190.80	375.50	447.00	474.10	554.10	657.40	751.20	883.40	1,002.10
Computational	178	205	396	473	501	583	687	782	921	1,035.00

practically observed by taking the difference of each modal frequency value between experimental and computational results. They arise due to complex manufacturing processes, design complexities, assembly stages and quality control issues. Consequently, when it comes to better optimization and increased performance, it is very important to mathematically analyze and incorporate uncertainties into the model. The coefficient of variation (CoV) is defined by Equation (8)

$$\text{CoV} = \frac{s_i}{\bar{x}_i}, i = 1, 2, \dots, 35 \quad (8)$$

where  $s_i$  denotes the standard deviation of 10 modal frequencies of each panel;  $\bar{x}_i$  denotes the average of 10 modal frequencies of each panel. Means and standard

deviations based on 10 modal frequency values are used to calculate the CoV for each AHSP sample. The results are tabulated in Table 7. The greatest variation is observed in Sample#29 (0.49) and the least variation is observed in Sample#6 (0.36). The AHSP and its estimated weight used for the computational stage are chosen using CoV statistics and a sampling scheme called bootstrap.

Based on the information obtained in the study, it is assumed that the errors are due to the uncertainties in the thickness of the upper and lower facing sheets and the thickness of the core cell wall. All three features are utilized to account for errors by running the PCE-Kriging model. However, before running the PCE-Kriging

**Table 5.** Errors between 35 experimental modal frequencies and the computational modal frequencies

Honeycomb #	Error=experimental value–computational value (in Hz)									
	1	2	3	4	5	6	7	8	9	10
1	-7.1	-9.4	-12.9	-17.0	-18.6	-22.2	-18.98	-14.98	-29.65	-16.20
2	-8.4	-9.3	-16.6	-17.2	-17.6	-20.0	-23.18	-20.68	-24.35	-26.10
3	-8.6	-10.8	-17.3	-20.6	-19.6	-26.7	-23.88	-21.88	-23.85	-24.40
4	-5.9	-7.0	-11.4	-13.1	-11.7	-16.7	-14.58	-12.08	-7.95	-9.90
5	-7.9	-8.6	-13.2	-18.0	-14.6	-19.9	-15.58	-16.28	-12.25	-9.20
6	-7.9	-8.6	-13.2	-18.0	-14.6	-19.9	-15.58	-16.28	-12.25	-9.20
7	-9.7	-11.8	-19.2	-22.8	-24.4	-27.5	-28.98	-31.78	-37.15	-39.80
8	-4.5	-5.8	-8.3	-11.9	-9.5	-12.1	-10.58	-6.68	-0.25	-1.90
9	-6.3	-6.8	-10.6	-15.2	-11.4	-15.5	-12.58	-12.18	-6.95	-6.60
10	-9	-10	-16	-23	-18	-23	-20.68	-20.48	-13.35	-16.40
11	-6	-7	-12	-17	-9	-15	-10.88	-13.88	4.75	-1.10
12	-4	-7	-10	-11	-11	-12	-11.98	-9.78	-7.15	-8.60
13	-9	-12	-18	-21	-25	-26	-26.98	-26.58	-37.15	-34.00
14	-8	-10	-15	-16	-20	-23	-23.08	-21.18	-31.05	-29.10
15	-6	-7	-10	-13	-14	-15	-13.68	-12.38	-15.15	-11.80
16	-8	-11	-18	-22	-18	-23	-22.68	-24.28	-21.75	-22.90
17	-7	-8	-13	-19	-16	-17	-17.48	-16.68	-9.55	-14.30
18	-7	-9	-14	-19	-16	-18	-20.48	-19.88	-21.45	-21.00
19	-9	-10	-16	-19	-18	-24	-23.38	-21.18	-23.35	-24.80
20	-11	-13	-21	-25	-25	-31	-29.88	-29.98	-35.55	-35.60
21	-11	-14	-23	-27	-27	-33	-33.58	-35.28	-36.05	-36.70
22	-10	-12	-18	-22	-24	-26	-27.68	-29.88	-32.75	-32.00
23	-11	-15	-23	-28	-31	-34	-37.58	-36.58	-48.95	-44.40
24	-10	-11	-19	-21	-23	-25	-31.48	-25.88	-29.05	-36.10
25	-18	-10	-18	-18	-19	-22	-24.58	-23.38	-23.75	-29.50
26	-9	-9	-15	-20	-13	-21	-20.68	-21.28	-15.25	-20.40
27	-9	-9	-17	-21	-15	-21	-20.18	-21.98	-14.85	-19.60
28	-10	-14	-21	-27	-24	-27	-27.58	-32.98	-36.65	-32.90
29	-10	-13	-20	-26	-23	-27	-25.48	-30.08	-27.45	-27.00
30	-8	-9	-16	-21	-15	-21	-19.58	-18.48	-7.85	-13.00
31	-8	-10	-14	-20	-21	-23	-21.38	-21.48	-23.05	-20.80
32	-6	-7	-11	-15	-13	-11	-14.28	-14.48	-1.15	-11.30
33	-8	-9	-17	-17	-17	-17	-23.38	-22.88	-13.25	-27.10
34	-7	-8	-14	-19	-16	-18	-17.68	-18.48	-12.85	-18.40
35	-10	-14	-20	-26	-27	-29	10.20	-30.88	-37.85	-32.90

model, ANOVA (Analysis of Variance) is run to check whether the errors of the 10 modal frequencies are statistically different. Otherwise, 10 different PCE-Kriging models need to be created. ANOVA is run at a significance level of 0.05 and a Duncan post hoc test is employed to determine which error of the 10 modal frequencies is statistically significant using SPSS version 27.0. The ANOVA results tabulated in Table 8 indicate that there are 3 groups. The results show that the least errors occur at modal frequencies #1 and #2, while the highest errors occur at modal frequencies #4 to #10. On the other hand, the error of modal frequency #3 appears to remain as a separate group.

**Table 6.** The statistical results

Weight (based on 10,000 samplings)	Bias
2,507.06	0.0996

The ANOVA result shows that 3 different OPCE-Kriging surrogate models need to be created to account for errors. UQ-Lab software [55] is used for all modeling processes. Leave-one-out (LOO) measure is used to determine how successful the model would be. Table 9 summarizes the coefficients of the three input variables and the LOO

**Table 7.** The coefficient of variations (CoV) of the 35 AHSP samples

AHSP#	CoV	AHSP#	CoV	AHSP#	CoV	AHSP#	CoV	AHSP#	CoV
1	0.48	8	0.48	15	0.43	22	0.49	29	0.49
2	0.48	9	0.45	16	0.41	23	0.42	30	0.45
3	0.49	10	0.41	17	0.45	24	0.48	31	0.42
4	0.55	11	0.43	18	0.40	25	0.43	32	0.45
5	0.41	12	0.47	19	0.45	26	0.42	33	0.44
6	0.36	13	0.47	20	0.45	27	0.39	34	0.46
7	0.42	14	0.41	21	0.37	28	0.40	35	0.42

**Table 8.** ANOVA results

Mode#	Group 1	Group 2	Group 3
10	-21.86		
6	-21.79		
8	-21.52		
9	-20.74		
7	-20.57		
4	-19.62		
5	-18.28		
3		-15.76	
2			-9.89
1			-8.44

**Table 9.** The results of PCE-Kriging models

Mode#	Lower facing sheet	Core cell wall thickness	Upper facing sheet	Optimization method	LOO
1-2	0.5185	0.2241	0.3831	Hybrid genetic algorithm	6.3725e-01
3	0.8031	3.4130	0.0529	Hybrid genetic algorithm	6.5984e-01
4 to 10	0.6516	9.8257	0.0156	Hybrid genetic algorithm	6.5484e-01

measure for each model and shows the results of the 3 models.

The three coefficients, lower facing sheet, core cell wall thickness and upper facing sheet, represent the contributions of the three stochastic variables to the errors between the experimental and computational 10 flexible mode frequency values. For modes #1 and #2, the first and third coefficients are larger than the second coefficient, indicating that errors occurring in these modes are more related to the facing sheets. Leave-one-out (LOO) is calculated for each model representing how many errors occurred when the prediction is conducted, and the value is 0.06. For modes #4 to #10, the second coefficient, core cell wall thickness, has a more dominant influence on the errors between experimental and computational values. Almost the same LOO value is attained by the predictions. Although the coefficient of the core structure is larger than the coefficients of the facing sheets, its dominance has just started to increase and is statistically different from modes #4 to #10, so it can be called a transition model for the errors. All models are optimized by UQLab using a Hybrid genetic

algorithm. Similarly, the LOO is around 0.06 in this model.

Thus, the results tabulated in Table 9 show that the lowest modes (mode#1 and mode#2) are dominated by upper and lower facing sheets, mode#4 and higher modes are dominated by the core structure. Mode#3 plays the transition role with a relatively higher core effect.

## 5. CONCLUSION

In this work, the dynamic response variability in 35 aluminum honeycomb sandwich panel (AHSP) samples are examined using a PCE and Kriging-based metamodel. The experimental data is acquired through experimental modal analysis (EMA) techniques. Accelerance frequency response functions (FRFs) are obtained at 21 predetermined locations in a response to the impulse response function generated by a modal hammer for every sample. The computational model is constructed using shell/shell/shell (SSS) modeling. As shown in a recent work [44], SSS modeling is statistically more successful in the prediction of the dynamic characteristics of AHSPs compared to the other two

modeling alternatives which are volume/volume/volume (VVV) and volume/shell/volume (SVS). The modal frequency values obtained for the first 10 flexible modes of the 35 samples are compared with the computational results and deviations are referred to as errors. Based on the information obtained in the study, it is assumed that the errors are due to uncertainties in the thicknesses of the upper and lower facing sheets and the thickness of the core cell wall. The outcomes of the study show that:

- The variability in the dynamic response of AHSPs increases with increasing frequency.
- The least variability occurs at low modal frequencies, mode#1, and mode#2, which are dominated by facing sheets rather than the core.
- The highest variability is observed at higher frequencies, mode#4 to mode#10, with an increasing trend. In this range the core is dominant.
- Mode#3 appears as a transition zone between the low frequency range, where the facing sheets dominate the dynamic response, and the high frequency range, where the core dominates the dynamic response.
- The dynamic response of the core walls is dominant in the high frequency region. As studies have shown, this response cannot be realized when the honeycomb core is taken as an equivalent volume [56–58].
- The uncertainties in the core structure mostly originated from the inhomogeneity of adhesive fillets which alter the effective cell wall thickness [22].
- In the relevant studies, it has been shown that the out-of-plane compressive strengths alter when the cell wall thickness value is changed at the junctions due the presence of adhesive fillets [59–61].

#### ACKNOWLEDGEMENT

This study was supported by Scientific and Technological Research Council of Turkey (TUBITAK) under the Grant Number 122M921. The authors thank TUBITAK for their supports.

#### DECLARATION OF ETHICAL STANDARDS

The authors of this manuscript declare that the materials and methods used in their studies do not require ethics committee approval and/or legal-specific permission.

#### AUTHORS' CONTRIBUTIONS

**Akm OKTAV:** Writing original draft, Computational and experimental analysis, Validation, Methodology, Funding acquisition.

**Murat Alper BAŞARAN:** Data curation, Investigation, Software, Conceptualization.

#### CONFLICT OF INTEREST

There is no conflict of interest in this study.

#### REFERENCES

- [1] Xiong J, Du Y, Mousanezhad D, Eydani Asl M, Norato J, Vaziri A., "Sandwich structures with prismatic and foam cores: A review", *Advanced Engineering Materials*, 21(1):1800036, (2019).
- [2] Tan HL, He ZC, Li KX, Li E, Cheng AG, Xu B., "In-plane crashworthiness of re-entrant hierarchical honeycombs with negative Poisson's ratio", *Composite Structures*, 1;229:111415, (2019).
- [3] Li QQ, Li E, Chen T, Wu L, Wang GQ, He ZC., "Improve the frontal crashworthiness of vehicle through the design of front rail", *Thin-Walled Structures*, 1;162:107588, (2021).
- [4] Tan H, He Z, Li E, Cheng A, Chen T, Tan X, Li Q, Xu B., "Crashworthiness design and multi-objective optimization of a novel auxetic hierarchical honeycomb crash box", *Structural and Multidisciplinary Optimization*, Oct;64(4):2009-24, (2021).
- [5] Xie S, Li H, Yang C, Yao S., "Crashworthiness optimisation of a composite energy-absorbing structure for subway vehicles based on hybrid particle swarm optimization", *Structural and Multidisciplinary Optimization*, 58:2291-308 (2018).
- [6] He W, Liu J, Wang S, Xie D., "Low-velocity impact response and post-impact flexural behaviour of composite sandwich structures with corrugated cores", *Composite Structures*, 1;189:37-53, (2018).
- [7] Bai Y, Wang N, Cheng P, Yu B, Badaruddin MF, Ashri M., "Collapse of Reinforced Thermoplastic Pipe (RTP) under external pressure", *International Conference on Offshore Mechanics and Arctic Engineering*, Jan 1 44366: 275-280 (2011).
- [8] Xiong J, Zhang M, Stocchi A, Hu H, Ma L, Wu L, Zhang Z., "Mechanical behaviors of carbon fiber composite sandwich columns with three-dimensional honeycomb cores under in-plane compression", *Composites Part B: Engineering*, Apr 1;60:350-8, (2014).
- [9] Wang X, Khodaparast HH, Shaw AD, Friswell MI, Zheng G., "Localisation of local nonlinearities in structural dynamics using spatially incomplete measured data", *Mechanical Systems and Signal Processing*, Jan 15;99:364-83, (2018).
- [10] Palomba G, Crupi V, Epasto G., "Collapse modes of aluminium honeycomb sandwich structures under fatigue bending loading", *Thin-Walled Structures*, Dec 1;145:106363, (2019).
- [11] Wang Z, Wang X, Liu K, Zhang J, Lu Z., "Crashworthiness index of honeycomb sandwich structures under low-speed oblique impact", *International Journal of Mechanical Sciences*, Oct 15;208:106683, (2021).
- [12] Palomba G, Epasto G, Crupi V. Lightweight sandwich structures for marine applications: a review. *Mechanics of Advanced Materials and Structures*. Oct 26;29(26):4839-64 (2022).
- [13] Sun Y, Li QM., "Dynamic compressive behaviour of cellular materials: A review of phenomenon, mechanism and modelling", *International Journal of Impact Engineering*, Feb 1;112:74-115 (2018).
- [14] Castanie B, Bouvet C, Ginot M., "Review of composite sandwich structure in aeronautic applications", *Composites Part C: Open Access* Aug 1;1:100004 (2020).
- [15] Qi C, Jiang F, Yang S., "Advanced honeycomb designs for improving mechanical properties: A review",

- Composites Part B: Engineering*, Dec 15;227:109393, (2021).
- [16] Boschetto A, Bottini L, Macera L, Vatanparast S., "Additive Manufacturing for Lightweighting Satellite Platform", *Applied Sciences*, Feb 22;13(5):2809, (2023).
- [17] Zhang X, Zhou H, Shi W, Zeng F, Zeng H, Chen G., "Vibration tests of 3D printed satellite structure made of lattice sandwich panels", *AIAA Journal*, Oct;56(10):4213-7, (2018).
- [18] Lionnet C, Lardeur P., "A hierarchical approach to the assessment of the variability of interior noise levels measured in passenger cars", *Noise Control Engineering Journal*, Jan 1;55(1):29-37, (2007).
- [19] Oktav A, Anlaş G, Yılmaz Ç., "Assessment of vehicle noise variability through structural transfer path analysis", *International Journal of Vehicle Design*, 71(1-4):300-20, (2016).
- [20] Oberkampf WL, Roy CJ., "Verification and validation in scientific computing", *Cambridge University Press* (2010).
- [21] Begg SH, Welsh MB, Bratvold RB., "Uncertainty vs. Variability: What's the Difference and Why is it Important?", *SPE Hydrocarbon Economics and Evaluation Symposium* May 19 (p. D011S003R002). SPE, (2014).
- [22] Oktav A., "Determination of the effect of adhesive fillets and viscous damping on the dynamic response of aluminum honeycomb sandwich panels", *Mechanics of Advanced Materials and Structures*, Sep 23:1-11, (2023).
- [23] Dai X, Shao X, Ma C, Yun H, Yang F, Zhang D., "Experimental and numerical investigation on vibration of sandwich plates with honeycomb cores based on radial basis function", *Experimental Techniques*, Feb;42:79-92 (2018).
- [24] Wang YJ, Zhang ZJ, Xue XM, Zhang L., "Free vibration analysis of composite sandwich panels with hierarchical honeycomb sandwich core", *Thin-Walled Structures*, Dec 1;145:106425, (2019).
- [25] Pourriahi V, Heidari-Rarani M, Torabpour Isfahani A., "Influence of geometric parameters on free vibration behavior of an aluminum honeycomb core sandwich beam using experimentally validated finite element models", *Journal of Sandwich Structures & Materials*, Feb;24(2):1449-69, (2022).
- [26] Rahman H, Jamshed R, Hameed H, Raza S., "Finite element analysis (FEA) of honeycomb sandwich panel for continuum properties evaluation and core height influence on dynamic behavior", *Advanced Materials Research*, Oct 1; 326:1-0, (2011).
- [27] Aborehab A, Kassem M, Nemnem A, Kamel M., "Miscellaneous modeling approaches and testing of a satellite honeycomb sandwich plate", *Journal of Applied and Computational Mechanics*, Dec 26, (2019).
- [28] Wang JT, Wang CJ, Zhao JP., "Frequency response function-based model updating using Kriging model", *Mechanical Systems and Signal Processing*, Mar 15;87:218-28, (2017).
- [29] Zhao Z, Wang H, Liu C, Xu X, Sun L, Wang J, Li Y., "An FFT-based method for uncertainty quantification of Nomex honeycomb's in-plane elastic properties", *Composite Structures*, Dec 1;301:116217, (2022).
- [30] Dey S, Mukhopadhyay T, Naskar S, Dey TK, Chalak HD, Adhikari S., "Probabilistic characterisation for dynamics and stability of laminated soft core sandwich plates", *Journal of Sandwich Structures & Materials*, Jan;21(1):366-97, (2019).
- [31] Zhang F, Du R, Qiao Z, Wang W, Zhang J, Wang X., "Quantitative structural uncertainty analysis of composite honeycomb sandwich using a feedback neural network", *Physica D: Nonlinear Phenomena*, Nov 9:133985, (2023).
- [32] Lajili R, Chikhaoui K, Zergoune Z, Bouazizi ML, Ichchou MN., "Impact of the vibration measurement points geometric coordinates uncertainties on two-dimensional k-space identification: Application to a sandwich plate with honeycomb core", *Mechanical Systems and Signal Processing*, Mar 15;167:108509, (2022).
- [33] Cheng YC, Yeh HC, Lee CK., "Multi-objective optimization of the honeycomb core in a honeycomb structure using uniform design and grey relational analysis", *Engineering Optimization*, Feb 1;54(2):286-304, (2022).
- [34] Dutta S, Ghosh S, Inamdar MM., "Optimisation of tensile membrane structures under uncertain wind loads using PCE and kriging based metamodels", *Structural and Multidisciplinary Optimization*, Mar;57:1149-61, (2018).
- [35] Dutta S., "A sequential metamodel-based method for structural optimization under uncertainty", *Structures*, 26:54-65, (2020).
- [36] Denimal E, Sinou JJ., "Advanced kriging-based surrogate modelling and sensitivity analysis for rotor dynamics with uncertainties", *European Journal of Mechanics-A/Solids*, Nov 1;90:104331, (2021).
- [37] Sudret B., "Global sensitivity analysis using polynomial chaos expansions", *Reliability Engineering & System Safety*, Jul 1;93(7):964-79, (2008).
- [38] Blatman G, Sudret B., "Adaptive sparse polynomial chaos expansion based on least angle regression", *Journal of Computational Physics*, Mar 20;230(6):2345-67 (2011).
- [39] Kleijnen JP., "Kriging metamodeling in simulation: A review", *European Journal of Operational Research*, Feb 1;192(3):707-16, (2009).
- [40] Rasmussen CE, Williams CK., "Gaussian processes for machine learning", *Cambridge, MA: MIT press*, (2006).
- [41] Possenti KA, de Menezes VG, Vandepitte D, Tita V, Medeiros RD., "Detection of changes in dynamic characteristics of composite structures using Kriging metamodeling procedure: Experimental and computational analysis", *Mechanics of Advanced Materials and Structures*, Aug 8:1-18, (2023).
- [42] Schwarz BJ, Richardson MH., "Experimental modal analysis", *CSI Reliability*, Oct 4;35(1):1-2, (1999).
- [43] Avitabile P., "Modal testing: a practitioner's guide", *John Wiley & Sons* (2017).
- [44] Oktav A, Başaran MA, Darıcık F., "Dynamic response optimization of a thermoplastic composite sandwich beam under random vibration", *Mechanics of Advanced Materials and Structures*, Jun 19:1-14, (2023).
- [45] Altıgen Co., Türkiye [https://www.6genpanel.com.tr/page12.html#extHeader2\\_6-57](https://www.6genpanel.com.tr/page12.html#extHeader2_6-57) accessed on March 23rd, 2025.
- [46] Santner TJ, Williams BJ, Notz WI, Williams BJ., "The design and analysis of computer experiments", *New York: Springer* (2003).
- [47] Hadj Kacem M, El Hami A, Dammak K, Trabelsi H, Walha L, Haddar M., "Consideration of multi-variable

- uncertainty using the GPC method for the dynamic study of a two-stage gearbox of a wind turbine”, *Mechanics of Advanced Materials and Structures*, Oct 20:1-4., DOI: 10.1080/15376494.2022.2138650, (2022).
- [48] Umesh K, Ganguli R., “Material uncertainty effect on vibration control of smart composite plate using polynomial chaos expansion”, *Mechanics of Advanced Materials and Structures*, Aug 9;20(7):580-91, (2013).
- [49] Azrar A, Ben Said M, Azrar L, Aljinaidi AA., “Dynamic analysis of Carbon NanoTubes conveying fluid with uncertain parameters and random excitation”, *Mechanics of Advanced Materials and Structures*, May 19;26(10):898-913, (2019).
- [50] Peng X, Ye T, Li J, Wu H, Jiang S, Chen G., “Multi-scale uncertainty quantification of composite laminated plate considering random and interval variables with data driven PCE method”, *Mechanics of Advanced Materials and Structures*, Nov 19;28(23):2429-39, (2021).
- [51] Chen M, Zhang X, Pan G., “Data-driven approach for uncertainty quantification and risk analysis of composite cylindrical shells for underwater vehicles”, *Mechanics of Advanced Materials and Structures*, 14:1-5. DOI: 10.1080/15376494.2023.2190762, (2023).
- [52] Aversano G, D’Alessio G, Coussement A, Contino F, Parente A., “Combination of polynomial chaos and Kriging for reduced-order model of reacting flow applications”, *Results in Engineering*, Jun 1;10:100223, (2021).
- [53] García-Macías E, Ubertini F., “Real-time Bayesian damage identification enabled by sparse PCE-Kriging meta-modelling for continuous SHM of large-scale civil engineering structures”, *Journal of Building Engineering*, Nov 1;59:105004, (2022).
- [54] Sinou JJ, Denimal E., “Reliable crack detection in a rotor system with uncertainties via advanced simulation models based on kriging and Polynomial Chaos Expansion”, *European Journal of Mechanics-A/Solids*, Mar 1;92:104451, (2022).
- [55] Marelli S, Sudret B., “UQLab: A framework for uncertainty quantification in Matlab”, *Vulnerability, Uncertainty, and Risk: Quantification, Mitigation, and Management*, Jul 13: 2554-2563, (2014).
- [56] Li L, He Q, Jing X, Jiang Y, Yan D., “Study on three-point bending behavior of sandwich beams with novel auxetic honeycomb core”, *Materials Today Communications*, 35:106259, (2023).
- [57] Dai X, Ye H, Yang W, Qi J, Liu Y, Yuan T, Wang Y., “Mechanical behaviors of inner and outer sidewalls of honeycomb cores subjected to out-of-plane compression”, *Aerospace Science and Technology*, 127:107659, (2022).
- [58] Wang WJ, Zhang WM, Guo MF, Yang JS, Ma L., “Energy absorption characteristics of a lightweight auxetic honeycomb under low-velocity impact loading”, *Thin-Walled Structures*, 185:110577, (2023).
- [59] Keshavanarayana SR, Shahverdi H, Kothare A, Yang C, Bingenheimer J., “The effect of node bond adhesive fillet on uniaxial in-plane responses of hexagonal honeycomb core”, *Composité Structures*, 175:111-122, (2017).
- [60] Kendall P, Sun M, Wowk D, Mechefske C, Kim IY., “Experimental investigation of adhesive fillet size on barely visible impact damage in metallic honeycomb sandwich panels”, *Composites Part B: Engineering*, 184:107723, (2020).
- [61] Chen X, Yu G, Wang Z, Feng L, Wu L., “Enhancing out-of-plane compressive performance of carbon fiber composite honeycombs”, *Composite Structures*, 255:12984, (2021).